Title

Photonic Thin Films Assembled from Amphiphilic Cellulose Nanofibrils Displaying Iridescent Full-Colors

Journal

ACS Applied Bio Materials, 3(7)

ISSN

2576-6422

Authors

Xu, Xuezhu
Zhou, He
Zhou, Guofu
et al.

Publication Date

2020-07-20

DOI

10.1021/acsabm.0c00463

Peer reviewed

ACS APPLIED BIO MATERIALS

www.acsabm.org Article

Photonic Thin Films Assembled from Amphiphilic Cellulose Nanofibrils Displaying Iridescent Full-Colors

Xuezhu Xu, He Zhou, Guofu Zhou, and You-Lo Hsieh*

Cite This: *ACS Appl. Bio Mater.* 2020, 3, 4522−4530 Read Online

ACCESS | Metrics & More | Article Recommendations | Supporting Information

ABSTRACT: Self-assembly of nanoparticles (NPs) to form structural colors offers promising opportunities for developing electronic, optoelectronic, and magnetic devices. In this regard, we reported co-assembly of cellulose nanofibrils (CNFs) and graphene to produce colored thin films. We demonstrated that biomimetic iridescent "peacock feather"-like full-color thin films can be generated by simple evaporation of aqueous suspensions on a surface tension confined, optically symmetric indium tin oxide-coated polyethylene terephthalate substrate. Amphiphilic CNFs serve dual functions to attract hydrophobic graphene via van der Waals interactions and to disperse hydrophilically and anionically CNF-tethered graphene while regulating surface tension to induce capillary and Marangoni flows in the force fields and construct thickness variation during dewetting. These CNF−graphene thin films exhibit full-color patterns and function as tunable light and moisture actuators. This approach has high potential to be applied to assemble other metal or metal oxide NPs for fast, simple, and robust fabrication without involving any complex lithography and external fields.

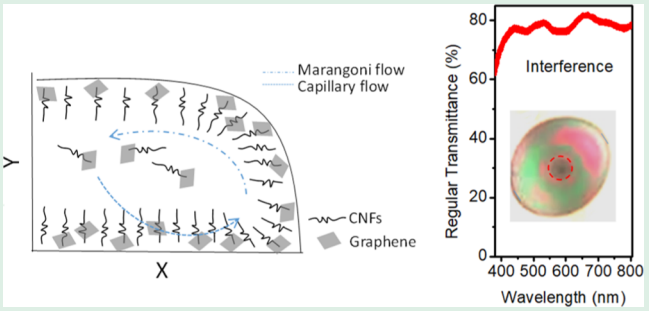

KEYWORDS: *structural color, photonic thin films, iridescence, cellulose nanofibrils, evaporation-induced self-assembly photonic thin films, amphiphilic cellulose nanofibrils, iridescent colors, light and moisture actuator*

1. INTRODUCTION

Thin films with spatially ordered sophisticated hierarchical structures, most commonly assembled from nanoparticles (NPs), have attracted much interest for their tailored electronic, magnetic, and optical properties[1] for a diverse range of applications in photovoltaics,[2] sensors,[3] catalysis,[4] and magnetic storage.[5] To date, organic or inorganic NPs in monodistributed sizes have been organized into ordered two-dimensional (2D) arrays by a myriad of techniques, including Langmuir−Blodgett deposition,[1] droplet evaporation,[6] and interfacial assembly.[7] In these approaches, NP assembly is generally known to be driven by attractive van der Waals interactions balanced by steric repulsion.[8] Depending on the competing effects of NP diffusion, convection, and solvent dewetting, a variety of patterns of 2D and three-dimensional (3D) ordered arrays as well as fractal aggregates, "coffee rings," photon crystals, and percolation clusters may emerge.[9] Thus, manipulating NPs and regulating their fluid interfaces may enable the formation of large ordered NP thin films.[10]

Among biologically derived nanomaterials, cellulose nanofibrils (CNFs) by (2,2,6,6-tetramethylpiperidin-1-yl)oxyl (TEMPO) oxidation first reported by de Nooy et al.[11] have been structured into 2D films and 3D gels.[12−18] While TEMPO-mediated oxidation regioselectively converts the surface C6 hydroxyls to carboxylate groups on CNFs, many pronounced attributes of high length-to-width aspect ratios,[19] low coefficient thermal expansion (3.8 ppm K^{-1}),[20] high tensile strength (1.6−6.4 GPa),[19] and Young's modulus (78−114 GPa),[21] as well as many versatile characteristics, such as reducing capability,[22] tunable softness,[23] gel−liquid phase transition,[24] binding ability,[25] dispersing character,[26] high transparency,[27] foaming ability,[28] and scaffolding[13] have also been discovered. We have derived various nanocelluloses from agricultural biomass by chemical and shear force methods.[29−31] The CNFs derived from rice straw by coupled TEMPO oxidation and shear force have shown to exhibit unique anisotropic amphiphilicity, because of exposure of the hydrophilic 110 and $1\bar{1}0$ as well as the hydrophobic 200 crystallographic planes of cellulose Iβ crystalline structure, to function as colloidal emulsifiers,[32] exfoliating dispersants for graphene,[26] and amphiphilic aerogels.[33] TEMPO-CNF from softwood bleached kraft has also been observed to sponta-

Received: April 23, 2020
Accepted: June 14, 2020
Published: June 15, 2020

https://dx.doi.org/10.1021/acsabm.0c00463
ACS Appl. Bio Mater. 2020, 3, 4522−4530

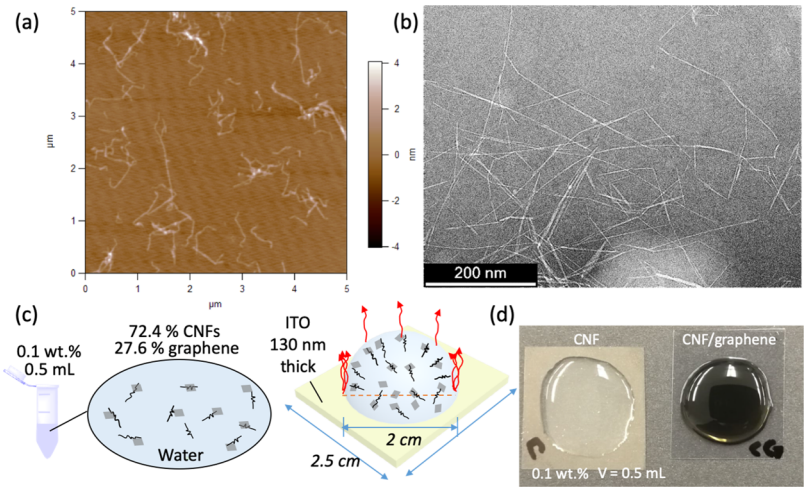

Figure 1. Morphologies of CNFs and CNF-containing suspensions: (a) AFM and (b) TEM images; (c) illustrations of aq. CNF-exfoliate graphene and deposition on ITO-coated PET; and (d) photographic images of 0.5 mL aq. CNF and CNF-exfoliate graphene on ITO-coated PET.

neously align into the plywood-like hierarchical structure to serve as an exceptionally high oxygen barrier film.[34]

To date, CNFs have been used as aqueous suspensions,[35] and widely made into fibers,[36] composites,[37] layer-by-layer films,[15] bulk films,[27] by varying processes of ambient drying,[38] wet spinning,[36] spin coating,[39] vacuum filtration,[27] and casting.[40] However, structural colors have only been observed on shorter, rigid rod-shape, and highly crystalline cellulose nanocrystals (CNCs) known for exhibiting chiral nematic pitch that displays colors in suspensions, thin films, and bulk films.[41,42] In CNC-silica composites, increasing silica contents have shown to increase the reflective wavelength λ_{max} to display a range of tunable colors like dark red, red, green, and blue[43] through evaporation-induced self-assembly (EISA).[44] Neutralizing CNC surface sulfates with strong Li^+, Na^+, K^+, NH^{4+}, NMe^{4+}, and NBu^{4+} containing bases could also retain intrinsic chiral nematic order in polar solvents, such as dimethyl sulfoxide, formamide, *N*-methylformamide, and dimethylformamide.[45] The particular photonic properties, that is, selective left-handed circularly polarized light reflection that pitches on the order of visible light wavelengths,[46,47] are of particular interest in physics. To our knowledge, self-assembly of CNFs to display structural colors has not been fully explored.

Here, we report the EISA of CNFs and iridescent microstructure of thin films showing intriguing photonic properties. This evaporation approach common to cast films from common polymers is simpler and more cost-effective than most processes reviewed. The optical activities and structural colors displayed by these CNF films are comparable with the self-assembled CNC but without the chiral nematic structure. The highly anisotropic amphiphilicity of the CNFs allowed them to bound to graphene and CNF-bound graphene to deposit on the hydrophobic substrate to function with flexibility, foldability, and fast response. As a proof-of-concept, we demonstrate the preparation of a family of iridescent CNF films whose optical properties can be easily tailored.

2. EXPERIMENTAL SECTION

2.1. Materials. Cellulose was extracted from rice straw (Calrose variety, harvested in California) using a three-step procedure, as reported previously.[30] Graphite flakes, toluene, anhydrous ethanol, sodium chlorite, acetic acid, potassium hydroxide, and sodium hypochlorite (NaClO) were used, as reported previously.[26] Sodium dodecyl sulfate (SDS, Sigma-Aldrich) was used as received. Indium tin oxide (ITO, 130 nm thick)-coated polyethylene terephthalate (PET, 0.127 mm thick) (Sigma-Aldrich) was used as the substrate for CNF coating. The ITO layer contained 90−100% diindium trioxide and 10−20% tin(IV) oxide. Silicon wafer featuring ⟨111⟩, P-type at 2 in. × 0.3 mm, was purchased from Sigma-Aldrich and used without further treatment. Water was purified by the Milli-Q plus water purification system (Millipore Corporate, Billerica, MA).

2.2. Preparation of CNF-Exfoliated Graphene and Thin Film. Aqueous CNF-exfoliated graphene (5 wt %) was prepared by aq. CNF with graphite flakes and blended (37×10^3 rpm) for 3 min and then centrifuged to collect the CNF-exfoliated graphene supernatant, as detailed previously.[26] To prepare CNF or CNF/graphene-coated ITO/PET films, aq. CNF or CNF-exfoliated graphene suspension (0.1 wt %, 0.5 mL) was drop-wise deposited onto ITO-coated PET and allowed to dry under ambient condition for 12 h. An ITO-coated PET substrate had a surface resistivity of 60 Ω/square and a root mean square roughness (R_q) of 0.856 ± 0.275 nm (5 μm × 5 μm) based on three atomic force microscopy (AFM) measurements.

2.3. Characterizations. AFM was performed using Asylum-Research MFP-3D, and transmission electron microscopy (TEM) was conducted using a JEOL2100F electron microscope. Scanning electron microscopy (SEM) imaging of dried graphene/CNF thin films (0.5 mL, 0.1%) on ITO/PET was performed on a Quattro S environmental scanning electron microscope from Fisher Scientific. Surface tension (γ) values were measured on a K10 Kruss tensiometer. CNF/graphene compositions were determined by graphene char quantity using a thermogravimetric analyzer (TGA-50, Shimadzu Company) operated at 10 °C min^{-1} rate to 500 °C. CNF and CNF/graphene show some decomposition below 200 °C, which was ascribed to the existence of absorbed moisture on TEMPO-oxidized CNF. Iridescent images of graphene/CNF thin films were taken by a polarizer-free camera (HAUPPAUGE winTV) equipped in the AFM. Profiles of dried films were scanned (0.074 μm/s resolution and 22.222 μm/s speed) by a Dektak XT 2D profilometer (Bruker). UV−vis spectra were collected on ∼1.6 cm diameter dried droplets (from 0.1 wt % graphene/CNF, 0.5 mL on ITO-coated PET) using a UV−vis spectrophotometer (Evolution 600, Thermo Scientific). Dynamic wetting profile of graphene/CNF droplets on substrates was imaged by a 1000× LED USB magnification digital microscope with a 0.3m CMOS image sensor and AMCAP—directshow software (version 9.0160).

Computation software COMSOL Multiphysics (version 5.3) with a wave optical module was used to model the microstructure−optics relationship, as assisted with the finite element method. A port boundary condition was included at the top. The port boundary condition at the top launched a plane wave at a specified angle at a

https://dx.doi.org/10.1021/acsabm.0c00463
ACS Appl. Bio Mater. 2020, 3, 4522−4530

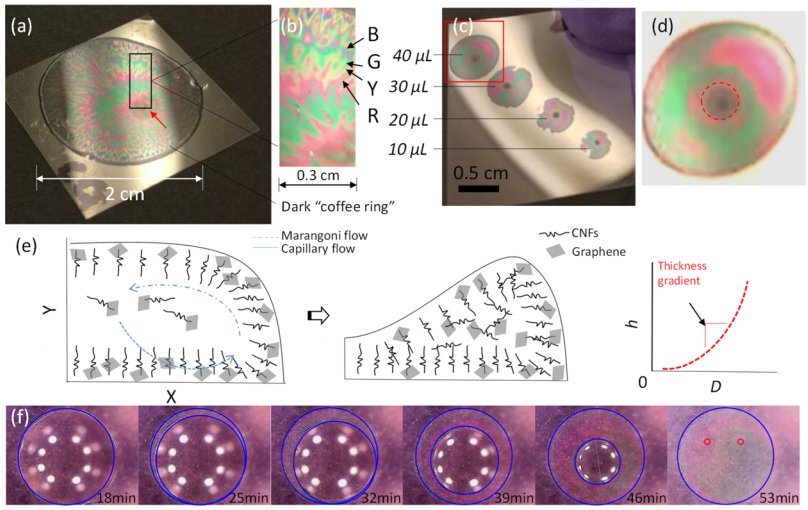

Figure 2. Air-dried aq. CNFs/graphene (0.5 mL, 0.1 wt %) on ITO-coated PET: (a) iridescent pattern formation dried tilted in the 4 o'clock direction as the dark spot showed; (b) close up of colors showing four basic colors (R: red; G: green; B: blue; and Y: yellow); (c) optical image by angular view (~60° to surface) of iridescent graphene/CNF (0.1%) films dried from various volumes of 40, 30, 20, and 10 μL; (d) optical image of a NP film (40 μL graphene/CNF dried on ITO/PET). Two concentric regions with distinct hues are visible. The inner region is a uniform NP monolayer (in dark) about 1 mm in diameter. The outer region contains contrary colors in red and green, which assemblies the appearance of a peacock's feather showing colorful eyespots; (e) sketch of EISA of aq. CNF/graphene on the ITO/PET substrate, showing amphiphilic CNFs with their hydrophobic sides/surfaces adhered to graphene and advanced by the capillary flow from center to edges. *D* and *h* [inset in (e)] denote distance from center to edge and film thickness, respectively; (f) top view of the wetting process of a 20 μL aq. 0.64% CNF suspension on an ITO/PET substrate, showing changes in contact lines and displaying of colors at the final stage (white dots were reflection of lamps).

certain incident power. Two interior boundaries were set to integrate the power flux in the upward and downward directions, then the total transmittance and reflectance could be obtained after being normalized by the incident power. Floquet periodic boundary condition was also included on the left and right sides for non-normal incident light.

3. RESULTS AND DISCUSSION

3.1. Formation of Iridescent Orderly Structure. The TEMPO-mediated oxidation coupled with high-speed blending (37,000 rpm) produced CNFs that were 1.69 ± 0.52 nm thick (n = 100) by AFM and 2.57 ± 0.85 nm wide and 0.99 ± 0.48 μm long (n = 200) by TEM (Figure 1a,b), which is consistent with previously reported findings from the same source and process.[48,49] As such measurements were made from dilute CNF concentrations on hydrophilic mica for AFM and glow-discharged grid for TEM, the wider surfaces along these substrates are assumed to be hydrophilic and those smaller surfaces along the height dimension to be hydrophobic. As reported previously, the hydrophobic CNF surfaces or the predominantly 200 crystallographic planes attach to graphite surfaces to aid aqueous exfoliation by high-speed shear force into exfoliated CNF-tethered graphene sheets at 84.2 wt % yield under an optimal 0.2 g/g graphene/CNF mass ratio.[26] Here, aqueous CNF/graphene (0.5 mL, 0.1 wt %) colloid was deposited onto a smooth (R_q = 0.856 ± 0.275 nm, Figure S1) ITO-coated PET substrate and then dried under the ambient condition (Figure 1c,d). Aqueous CNF alone was also prepared in the same manner for comparison.

Upon air drying under ambient condition, aq. CNF-tethered graphene or CNF/graphene (0.5 mL, 0.1 wt %, Figure 2a) deposited onto the ITO-coated PET substrate formed a thin coating covering a ca. 2 cm diameter area and appeared iridescent, showing blue, green, yellow, and red colors (Figure 2b). Graphene/CNF films containing 72.4 wt % CNFs (calculated from thermogravimetric analysis (TGA) data, Figure S2) had a dark perimeter and a black dot in the center (Figure 2a). When dried slightly tilted, the dark center of the iridescent circle drifted in the gravitational flow direction, as pointed by an arrowhead in Figure 2a. Comparatively, aqueous dispersions of graphene alone at either 0.2 or 0.002 wt % on ITO dried to gray, evenly spread, homogeneous thin films without colors (Figure S3), inferring the structural color to originate from CNFs rather than graphene. Such similar iridescent patterns were observed on all thin films containing CNF, that is, aq. CNF alone, or aq. graphene/CNF with 0.0067 to 0.067% CNF, dried at 25 or 50 °C, as well as in varying droplet volumes of 10, 20, 30, and 40 μL, showing theses structural colors to be independent of aq. CNF concentrations and volumes (Figure 2c). Clearly, the zoomed angular view of the film from 40 μL 0.1% graphene/CNF on ITO (Figure 2d) showed circular iridescent patterns mimicking the biologically structural coloration found on eyespots of peacock's train feather.

Interestingly, neither CNF bulk films nor CNF coatings have been reported to show orderly structures when fabricated by the vacuum filtration-assisted paper-making technique (Figure S4).[40,50] In fact, bacterial cellulose CNF/graphene, coated on the PET substrate,[50] appeared gray displaying no other colors. The rarely seen iridescent colors are thought to be related to surface tension (γ) caused by the unique amphiphilic nature of these CNFs, as sketched in Figure 2e. The CNF-tethered graphene sheets inside the droplet move upward from the perimeter along the air/liquid interface (Marangoni flow) and outward toward the edge along the liquid/solid interface (capillary flow) where γ is minimal at these interfaces, giving rise to the mass transport in the radiant direction. Marangoni flow is an anticapillary flow, which goes from edge to center at the air/liquid interface induced by the constantly changing and uneven surface tensions. Marangoni number (Ma) described contribution from two factors[51]

https://dx.doi.org/10.1021/acsabm.0c00463
ACS Appl. Bio Mater. 2020, 3, 4522−4530

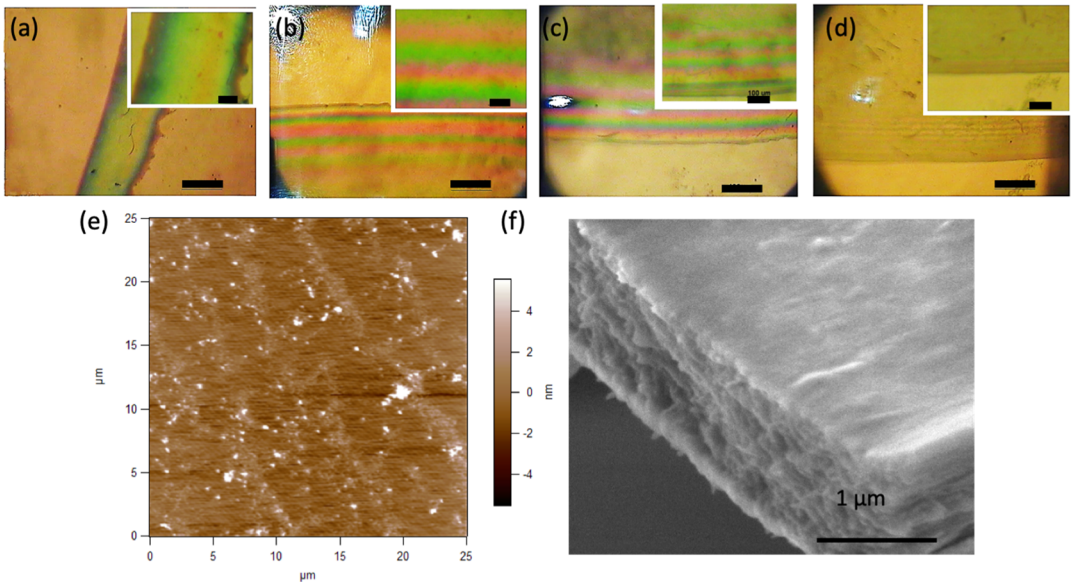

Figure 3. Microscopic images of CNF-only thin-film series cast from ambient drying of aq. CNF (0.00067−0.67%) on ITO-coated PET taken by a polarizer-free camera equipped in AFM: (a) 0.00067; (b) 0.0067; (c) 0.067; and (d) 0.67%. Images in (b,c) display the strongest iridescence. The scale bars in (a−d) were 150 μm; (e) AFM image of CNF/graphene; and (f) TEM image of cross-sectional and top views of a piece of CNF/graphene thin film detached from ITO/PET substrate.

$$Ma = -\mathrm{d}\gamma/\mathrm{d}t \times (\Delta TL/\eta\alpha)$$

where γ denotes the liquid surface tension, t is the time, ΔT is the temperature difference within the colloidal droplet, L is the characteristic droplet length, and η and α are the dynamic viscosity and thermal diffusivity of the droplet, respectively. The capillary flow transports either CNF or CNF-tethered graphene from center to edge. Along this process, the rate of evaporation is higher around the edges of the liquid/solid interface, increasing γ at the high-concentration CNF location (x-axis direction, Figure 2e), which accelerates the upward movement of CNFs toward the center along the air/liquid interface. The CNF-tethered graphene sheets flow radiantly toward the edge of the droplet via the capillary flow where they accumulate and solidify upon water evaporation, forming a gradient of thickness in a volcanic crater profile or "hills" in iridescence. Similar "coffee particulates," "silver nanowires," and monodispersed polystyrene have also shown to form volcanic crater shapes driven by an outward capillary flow from center to edge.[52,53]

Figure 2f presents the top view of a 20 μL aq. 0.64% CNF suspension on the ITO-coated PET substrate, showing changes in contact lines around the thin-film area. Initially, the drop size stayed unchanged until ca. t = 18 min (figure not shown here) and then shrunk when completely dried at t = 53 min. During the initial 18 min for the solvent in the CNF suspension to evaporate, CNFs undergo intensive movements because of Marangoni and capillary flows and flow-induced reorganization. Then, the contact line shrunk and vanishes from the edge to the center. The contact area reduced linearly with time (Figure S5), suggesting an even evaporating rate. What is worth noting, in the last image, a slight iridescent coloration is inversely located displaying red and green formed on the film, which indicated that there is possible relationship of the microstructure with viewing angles.

To find out the factors of the CNF concentration affecting the appearance of patterning, the as-prepared CNF suspension (0.67%) was diluted to a gradient of concentrations from 0.00067 to 0.67% and then 10 μL of each concentration deposited and air dried on the ITO-coated PET substrate. The strongest iridescent patterns were observed on those from 0.0067 to 0.067% CNF concentrations (Figure 3b,c). Clearly, the iridescence patterns originate from the self-organization of CNFs in the specific range of concentrations where sufficient CNFs and inter-CNF spacing allow such organization. The iridescence faded out on that at 0.67% aq. CNF that gelled, indicating limited reorganization of individual CNFs. In gelation, the critical percolation threshold φ_c, which characterizes formation of the network, equals to $0.7/(L/W)$, where L and W denote the respective average CNF length and width.[30,31,54] Based on CNF dimensions measured, φ_c is calculated to be 0.1817%, the CNF concentration above which the formation of the CNF network hinders their self-assembling. Therefore, iridescence is expected to be observed in films from aq. CNF at concentrations up to the 0.1817% percolation threshold which falls between the 0.067 and 0.67% observed. The 0.1% aq. graphene/CNF protocol contained 0.0724% CNF which was far below the 0.1817% percolation threshold φ_c, where free CNF−CNF colloidal interactions and assembling could result in an orderly structure with an iridescent texture.

The AFM image of the CNF/graphene thin-film surfaces coated on either mica or the ITO/PET substrate showed no clear evidence of fibril alignment (Figures 3e and S6), suggesting the preferential surfacing of graphene to reduce surface tension. The cross-sectional CNF/graphene thin film showed no evidence of chiral pitch (Figure 3f). During this process, obvious Newton's rings emerge on the thin film because of the rapid and uniform thinning of the several micron thick aq. suspension into near 100 nm thick film. As thinning progresses, CNFs or CNF-tether graphene sheets in the suspension adhere to the substrate and cannot move in the thin film. Finally, as the Newton's rings disappear, a radially oriented alignment of CNF or CNF/graphene array is left on the substrate.

https://dx.doi.org/10.1021/acsabm.0c00463
ACS Appl. Bio Mater. 2020, 3, 4522−4530

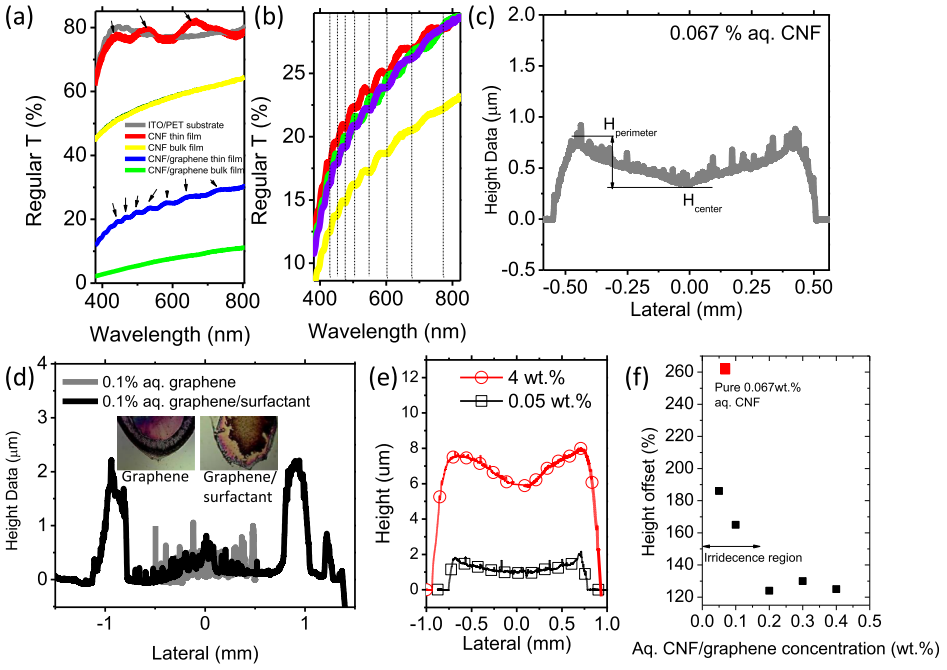

Figure 4. Optical properties and topological microstructures of CNF and CNF/graphene thin films on the ITO/PET substrate: (a) UV−vis spectra of films and their bulk counterparts; (b) UV−vis spectra of several arbitrarily selected locations in films; (c) topological microstructures of CNF thin films on the ITO/PET substrate scanned by a profiler; (d) graphene thin films on the hydrophobic substrate (silicone) prepared from 0.1 wt % aq. graphene suspension alone or that stabilized by 0.3 wt % SDS; (e) topological microstructures on two representatives, including thick (4 wt %) and thin (0.05 wt %) CNF/graphene films; and (f) height offset vs aq. CNF/graphene concentrations, the arrow marked the concentration range (<0.2 wt %) displaying structural colors. Red square denoted the film derived from pure 0.067 wt % CNF displaying colors.

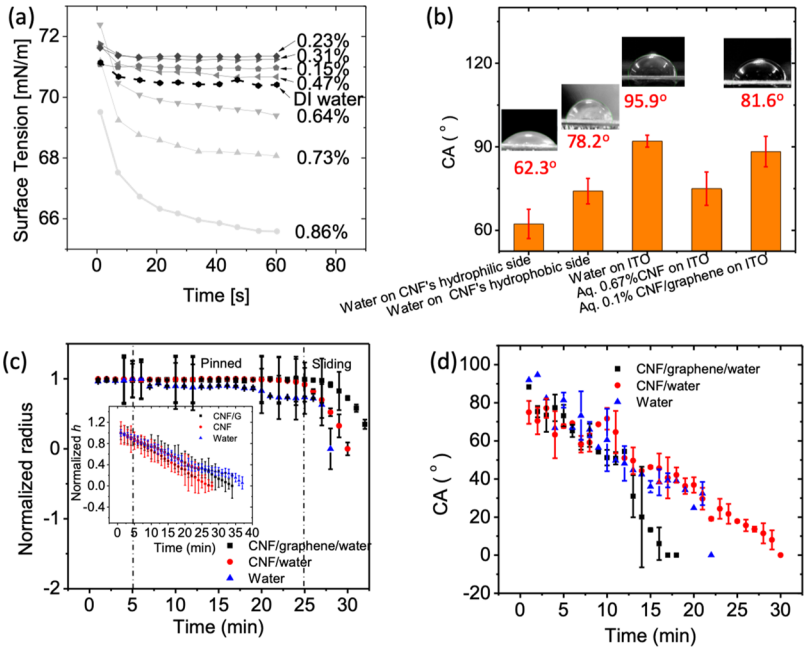

Figure 5. Wetting dynamics of aq. graphene/CNF (0.1%) on ITO with water and aq. CNF (0.23−0.067%) for comparison: (a) time-lapse variation in surface tension (γ) of aq. CNF suspensions at 0−0.86% CNF concentrations. Lower left inset depicts the height and radius change as water evaporates, upper right inset proposes CNF moves at different times; (b) CAs of a 10 μL water or aq. CNF sessile droplets on the ITO substrate; and (c) normalized droplet radius and heights (inset) of above-mentioned liquid droplets. Normalization was dealt by transforming data vector into a new vector whose norm (i.e., h, radius) equals to 1. (d) Time-lapse changes in CA of 10 μL CNF (0.067%), graphene/CNF (0.1%), and water on ITO.

3.2. Optical Properties and Volcanic Mouth Microstructure of CNF-Containing Thin Films. Light transmittance of CNF and graphene/CNF thin films evaporated from aq. suspensions (0.5 mL, 0.1%) on top of the ITO-coated PET substrate was compared with that of their bulk films (~15 μm thick) prepared by vacuum filtration (Figure 4a) and at several arbitrarily selected locations of graphene/CNF thin film on the ITO/PET substrate (Figure 4b). The ITO-coated PET

https://dx.doi.org/10.1021/acsabm.0c00463
ACS Appl. Bio Mater. 2020, 3, 4522−4530

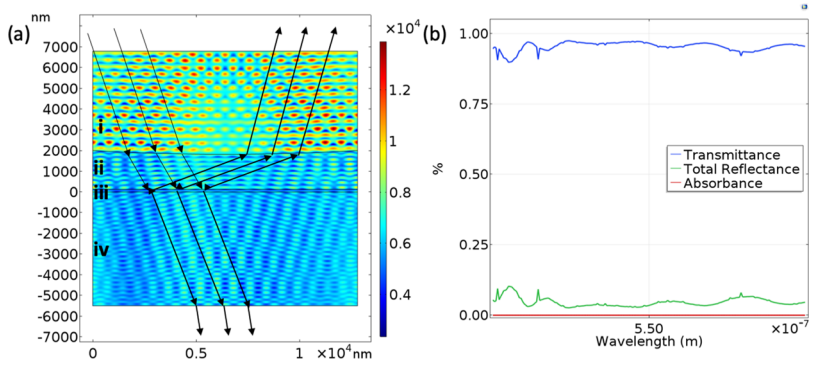

Figure 6. COMSOL modeling to predict the optical activity of multiple layers of CNF-coated ITO/PET with the Roman numbers denoting each layer material, (i): air; (ii): CNFs; (iii): ITO; and (iv): PET: (a) computational model of the layered microstructure with the CNF layer having a radius of 12 μm, radius of curvature of 115 μm, and a height of 4 μm and (b) computational modeled results for optical transmittance, reflectance, and absorbance of CNF-containing triple layers.

substrate transmitted up to ~80% in the visible light spectra in an unremarkably smooth line. Intriguingly, both graphene/CNF and CNF thin films on the ITO-coated PET substrate exhibited multiple peaks throughout the visible light spectrum, clearly indicating the presence of optical interference. Neither bulk films showed any specific UV−vis absorption, suggesting the colors to be originating from thin-film-air surface and interfaces to be elucidated in the following section.

To further examine the microstructure-induced optical phenomenon, a dilute aq. CNF droplet (0.067%, 10 μL) was dried on a rigid hydrophobic silicon wafer surface to also form ca. 1 mm diameter circular thin films with unique volcano-shaped thickness contour of 0.884 μm perimeter height and 0.337 μm height in the center or a 262% height offset ($H_{perimeter}/H_{center} \times 100\%$) (Figure 4c). In contrast, both 0.1% aq. graphene and 0.1% aq. graphene/SDS suspensions deposited onto ITO dried into thin films in even thickness without any colorful pattern at all (Figure 4d). Similar to CNF alone, graphene/CNF droplets (20 μL) at 0.05, 0.1, 0.2, 0.3, and 0.4% concentrations dried on ITO also exhibited volcanic thickness profiles with respective 186, 165, 124, 130, and 125% height offsets, of which the representative 0.05 and 0.4% curves are shown in Figure 4e. Observation with the naked eyes, those from the lower 0.05−0.1% graphene/CNF concentrations appeared iridescent but not as strong as those from 0.2 to 0.4% concentrations (Figure 4f). It is very clear that the iridescence is attributed to CNF only, not graphene; only CNF-containing suspensions, that is, graphene/CNF or CNF, deposited on ITO series, are dried to volcanic-shaped thickness profiles that were not observed on those obtained from aq. graphene suspensions. The distinct iridescent phenomenon is attributed to the Bragg reflection in the gradient slope microstructured thin film of self-assembled CNFs driven by differential water evaporation (Marangoni flow) and surface tension (capillary flow) in aq. liquid deposited onto hydrophobic ITO-coated substrates, which is not observed in thick bulk films.

3.3. Dynamic Wetting Related to Self-Assembling Mechanism of CNFS. How the amphiphilic characteristics of CNF surfaces affect their aq. suspension behaviors was further probed by their effects on water surface tension and dewetting behaviors. With increasing CNF concentrations from 0.23 to 0.86 wt %, the surface tension γ (70.4 mN m^{-1}) first increased slightly to 71.3 mN m^{-1} with 0.23 wt % CNF, then decreased to 65.7 mN m^{-1} as the CNF concentration further increased to 0.86 wt % (Figure 5a). This is consistent with the anisotropic and amphiphilic characteristics of CNFs that have shown to aid aqueous exfoliation and stabilization of bound graphene.[26] The anisotropic CNF surface amphiphilicity can also be reflected in their film surfaces. Neat CNF thin film dried from 0.3% aq. CNF on the hydrophobic ITO had a static water contact angle (CA) of 62.3° on the surface exposed to air and 78.2° on the surface dried facing the hydrophobic ITO (Figure 5b), reflecting the nature of the air and ITO surfaces CNF exposed. Water formed a CA of 91.9° on the hydrophobic ITO, a lowered CA of ~74.9° on CNF and raised CA back to ~81.6° on the more hydrophobic graphene/CNF, the effects expected from amphiphilic CNFs and hydrophobic graphene/CNF. These observations support the notion that amphiphilic CNFs rotate to lower the surface tension with respect to the specific interfaces. For a liquid droplet on a surface, the height (h) is associated with the radius R and CA (θ): $h = R \tan(\theta/2)$.[51] The radius for both aq. CNF and graphene/CNF remained unchanged at 1 (normalized) for ~25 min, then drastically reduced (Figure 5c), which is obviously different from the constant decreasing radius of pure water. Meanwhile, the h and CA of both aq. CNF and graphene/CNF decreased linearly with time (Figure 5d). That the radius remained constant till t = 25 min suggests aq. CNF-containing droplet on hydrophobic ITO resembled a constant contact area motion, that is, pinned contacting area between the liquid/substrate but decreasing CA and h with time as a function of decreasing dynamic surface tension with the increasing concentration or evaporation.

Computational modeling by COMSOL software confirmed our prediction that optical interference of irradiative light with CNF/ITO/PET resulted in the structural colors. As shown in Figure 6a, we built from top to bottom a structure with air (i) CNFs (ii), ITO (iii), and PET (iv) filled in each layer. Incident light came at a 661 nm wavelength shining at 60° angle from the top. Each layer has a thickness very close to that of experimentally prepared thin film, that is, the CNF layer has a concave dent at a 12 μm radius, a 115 μm radius of curvature of 115 μm, and a height of 4 μm (from the highest to lowest), comparing to 0.067% CNF coated on a silicon surface to form 1 mm diameter, volcano-shaped contour of 0.884 μm perimeter height, and 0.337 μm height in the center (Figure 4c). Some discernments were set because of the limitation of computations. The refractive index for air and PET was set at 1.0003 and 1.6357, respectively, while interpolation curves were introduced to describe the wavelength-dependent

https://dx.doi.org/10.1021/acsabm.0c00463
ACS Appl. Bio Mater. 2020, 3, 4522−4530

refractive index of CNF and ITO. Using the transfer-matrix method, the computational modeled results are shown in Figure 6b for optical transmittance, reflectance, and absorbance of CNF-containing triple layers. We observed that the incident light also generated wavy curves, which is believed to attribute to the above-mentioned Bragg refraction within the layers. The optical properties of bulk CNF films with a thickness of > 10 μm were also computed but did not show the wavy peaked curves, confirming the role of the nanometer structure in generation of interference. In summary, the color of these films is caused by the thin-film interference because of the thickness variation.

4. CONCLUSIONS

Unique photonic structures displaying bright iridescent full-color patterns have been facilely built from air drying of aq. CNF alone or CNF-tether graphene at 0.0067−0.067% deposited onto the ITO-coated PET substrate. The concentric microstructure and volcanic crater contour were driven by Marangoni and capillary flows of amphiphilic CNF alone and with tethered graphene. The thickness variation induced a complex optical pathway, which caused the formation of sizable, colorful, iridescent full structural colors, as confirmed by computational modeling.

This proof-of-concept study shows that this approach of surface-energy-assisted aq. CNF coating and ambient drying provides sufficient control over the flow of liquid droplets to define sizable critical features. The unique amphiphilicity of the biologically derived CNF nanomaterial to function as a structural color material is particularly significant for its easy assembling, high scalability, and sustainability in a variety of technology areas. As demonstrated with graphene, other NPs, such as carbon nanotubes and inorganic noble metals, may also be coupled with CNFs for structural patterning and, upon calcination to remove the template, used as electrodes. These sizable photonic thin films may find applications in camouflage coatings, optical filters, solar gain regulators, reflective displays, negative refraction, and superlens.

■ ASSOCIATED CONTENT

Supporting Information

The Supporting Information is available free of charge at https://pubs.acs.org/doi/10.1021/acsabm.0c00463.

Surface roughness of CNF/graphene on ITO-PET by AFM; TGA of CNF/graphene, CNF, and graphene; photograph of graphene on ITO-PET and glass; photograph of bacterial cellulose CNF/graphene on PET; contact area of aq. CNF on ITO-PET; and AFM of CNF/graphene on ITO/PET (PDF)

■ AUTHOR INFORMATION

Corresponding Author

You-Lo Hsieh − *Biological and Agricultural Engineering, University of California, Davis, California 95616, United States;* orcid.org/0000-0003-4795-260X; Phone: +1 530 752 0843; Email: ylhsieh@ucdavis.edu; Fax: +1 530 752 7584

Authors

Xuezhu Xu − *Biological and Agricultural Engineering, University of California, Davis, California 95616, United States; Guangdong Provincial Key Laboratory of Optical Information Materials and Technology, Institute of Electronic Paper Displays, South China Academy of Advanced Optoelectronics, South China Normal University, Guangzhou 510006, China*

He Zhou − *Guangdong Provincial Key Laboratory of Optical Information Materials and Technology, Institute of Electronic Paper Displays, South China Academy of Advanced Optoelectronics, South China Normal University, Guangzhou 510006, China*

Guofu Zhou − *Guangdong Provincial Key Laboratory of Optical Information Materials and Technology, Institute of Electronic Paper Displays, South China Academy of Advanced Optoelectronics, South China Normal University, Guangzhou 510006, China;* orcid.org/0000-0003-1101-1947

Complete contact information is available at: https://pubs.acs.org/10.1021/acsabm.0c00463

Notes

The authors declare no competing financial interest.

■ ACKNOWLEDGMENTS

The authors appreciate the support from the California Rice Research Board (Project RU-9) as well as the National Key R&D Program of China (no. 2016YFB0401501), Program for Chang Jiang Scholars and Innovative Research Teams in Universities (no. IRT 17R40), Guangdong Provincial Key Laboratory of Optical Information Materials and Technology (no. 2017B030301007), Ministry of Education (MOE) International Laboratory for Optical Information Technologies, and 111 Project.

■ REFERENCES

(1) Heath, J. R.; Knobler, C. M.; Leff, D. V. Pressure/Temperature Phase Diagrams and Superlattices of Organically Functionalized Metal Nanocrystal Monolayers: The Influence of Particle Size, Size Distribution, and Surface Passivant. *J. Phys. Chem. B* **1997**, *101*, 189−197.

(2) O'Regan, B. O.; Gratzelt, M. A Low-Cost, High-Efficiency Solar Cell Based on Dye-Sensitized Colloidal $Ti0_2$ Films. *Nature* **1991**, *353*, 737−740.

(3) Jiang, C.; Markutsya, S.; Pikus, Y.; Tsukruk, V. V. Freely Suspended Nanocomposite Membranes as Highly Sensitive Sensors. *Nature* **2004**, *3*, 721−728.

(4) Haruta, M. Gold as a novel catalyst in the 21st century: Preparation, working mechanism and applications. *Gold Bull.* **2004**, *37*, 27−36.

(5) Sun, S.; Murray, C. B.; Weller, D.; Folks, L.; Moser, A. Monodisperse FePt Nanoparticles and Ferromagnetic FePt Nanocrystal Superlattices. *Science* **2000**, *287*, 1989−1993.

(6) Motte, L.; Billoudet, F.; Lacaze, E.; Douin, J.; Pileni, M. P.; Laboratoire, S. R. S. I.; Uni, V. Self-Organization into 2D and 3D Superlattices of Nanosized Particles Differing by Their Size. *J. Phys. Chem. B* **1997**, *101*, 138−144.

(7) Mueggenburg, K. E.; Lin, X.-M.; Goldsmith, R. H.; Jaeger, H. M. Elastic Membranes of Close-Packed Nanoparticle Arrays. *Nature* **2007**, *6*, 656−660.

(8) Narayanan, S.; Wang, J.; Lin, X. Dynamical Self-Assembly of Nanocrystal Superlattices during Colloidal Droplet Evaporation by in Situ Small Angle X-Ray Scattering. *Phys. Rev. Lett.* **2004**, *93*, 135503.

(9) Redl, F. X.; Cho, K.; Murray, C. B.; Brien, S. O. Three-Dimensional Binary Superlattices of Magnetic Nanocrystals and Semiconductor Quantum Dots. *Nature* **2003**, *423*, 968−971.

(10) Santhanam, V.; Liu, J.; Agarwal, R.; Andres, R. P. Self-Assembly of Uniform Monolayer Arrays of Nanoparticles. *Langmuir* **2003**, *19*, 7881−7887.

(11) de Nooy, A. E. J.; Besemer, A. C.; van Bekkum, H. Highly selective tempo mediated oxidation of primary alcohol groups in polysaccharides. *Red. Trav. Chim. Pays-Bas* **1994**, *113*, 165−166.
(12) Wang, B.; Benitez, A. J.; Lossada, F.; Merindol, R.; Walther, A. Bioinspired Mechanical Gradients in Cellulose Nanofibril/Polymer Nanopapers. *Angew. Chem., Int. Ed.* **2016**, *55*, 5966−5970.
(13) Olsson, R. T.; Azizi Samir, M. A. S.; Salazar-Alvarez, G.; Belova, L.; Ström, V.; Berglund, L. A.; Ikkala, O.; Nogués, J.; Gedde, U. W. Making Flexible Magnetic Aerogels and Stiff Magnetic Nanopaper Using Cellulose Nanofibrils as Templates. *Nat. Nanotechnol.* **2010**, *5*, 584−588.
(14) Cai, J.; Liu, S.; Feng, J.; Kimura, S.; Wada, M.; Kuga, S.; Zhang, L. Cellulose-Silica Nanocomposite Aerogels by In Situ Formation of Silica in Cellulose Gel. *Angew. Chem., Int. Ed.* **2012**, *51*, 2076−2079.
(15) Karabulut, E.; Pettersson, T.; Ankerfors, M.; Wågberg, L. Adhesive Layer-by-Layer Films of Carboxymethylated Cellulose Nanofibril-Dopamine Covalent Bioconjugates Inspired by Marine Mussel Threads. *ACS Nano* **2012**, *6*, 4731−4739.
(16) Fukuzumi, H.; Saito, T.; Isogai, A. Influence of TEMPO-Oxidized Cellulose Nanofibril Length on Film Properties. *Carbohydr. Polym.* **2013**, *93*, 172−177.
(17) Wu, Z.-Y.; Li, C.; Liang, H.-W.; Chen, J.-F.; Yu, S.-H. Ultralight, Flexible, and Fire-Resistant Carbon Nanofiber Aerogels from Bacterial Cellulose. *Angew. Chem.* **2013**, *125*, 2997−3001.
(18) Shopsowitz, K. E.; Qi, H.; Hamad, W. Y.; MacLachlan, M. J. Free-Standing Mesoporous Silica Films with Tunable Chiral Nematic Structures. *Nature* **2010**, *468*, 422−425.
(19) Saito, T.; Kuramae, R.; Wohlert, J.; Berglund, L. A.; Isogai, A. An Ultrastrong Nanofibrillar Biomaterial: The Strength of Single Cellulose Nanofibrils Revealed via Sonication-Induced Fragmentation. *Biomacromolecules* **2013**, *14*, 248−253.
(20) Shimizu, M.; Fukuzumi, H.; Saito, T.; Isogai, A. Preparation and Characterization of TEMPO-Oxidized Cellulose Nanofibrils with Ammonium Carboxylate Groups. *Int. J. Biol. Macromol.* **2013**, *59*, 99−104.
(21) Guhados, G.; Wan, W.; Hutter, J. L. Measurement of the Elastic Modulus of Single Bacterial Cellulose Fibers Using Atomic Force Microscopy. *Langmuir* **2005**, *21*, 6642−6646.
(22) Dong, H.; Snyder, J. F.; Tran, D. T.; Leadore, J. L. Hydrogel, Aerogel and Film of Cellulose Nanofibrils Functionalized with Silver Nanoparticles. *Carbohydr. Polym.* **2013**, *95*, 760−767.
(23) Capadona, J. R.; Shanmuganathan, K.; Tyler, D. J.; Rowan, S. J.; Weder, C. Stimuli-Responsive Polymer Nanocomposites Inspired by the Sea Cucumber Dermis. *Science* **2008**, *319*, 1370−1374.
(24) Dong, H.; Snyder, J. F.; Williams, K. S.; Andzelm, J. W. Cation-Induced Hydrogels of Cellulose Nanofibrils with Tunable Moduli. *Biomacromolecules* **2013**, *14*, 3338−3345.
(25) Lu, H.; Behm, M.; Leijonmarck, S.; Lindbergh, G.; Cornell, A. Flexible Paper Electrodes for Li-Ion Batteries Using Low Amount of TEMPO-Oxidized Cellulose Nanofibrils as Binder. *ACS Appl. Mater. Interfaces* **2016**, *8*, 18097−18106.
(26) Xu, X.; Hsieh, Y.-L. Aqueous exfoliated graphene by amphiphilic nanocellulose and its application in moisture-responsive foldable actuators. *Nanoscale* **2019**, *11*, 11719−11729.
(27) Huang, J.; Zhu, H.; Chen, Y.; Preston, C.; Rohrbach, K.; Cumings, J.; Hu, L. Highly Transparent and Flexible Nanopaper Transistors. *ACS Nano* **2013**, *7*, 2106−2113.
(28) Wicklein, B.; Kocjan, A.; Salazar-Alvarez, G.; Carosio, F.; Camino, G.; Antonietti, M.; Bergström, L. Thermally Insulating and Fire-Retardant Lightweight Anisotropic Foams Based on Nanocellulose and Graphene Oxide. *Nat. Nanotechnol.* **2014**, *10*, 277−283.
(29) Lu, P.; Hsieh, Y.-L. Preparation and Characterization of Cellulose Nanocrystals from Rice Straw. *Carbohydr. Polym.* **2012**, *87*, 564−573.
(30) Jiang, F.; Hsieh, Y.-L. Chemically and Mechanically Isolated Nanocellulose and Their Self-Assembled Structures. *Carbohydr. Polym.* **2013**, *95*, 32−40.
(31) Jiang, F.; Han, S.; Hsieh, Y.-L. Controlled Defibrillation of Rice Straw Cellulose and Self-Assembly of Cellulose Nanofibrils into Highly Crystalline Fibrous Materials. *RSC Adv.* **2013**, *3*, 12366.
(32) Jiang, F.; Hsieh, Y.-L. Holocellulose Nanocrystals: Amphiphilicity, Oil/Water Emulsion, and Self-Assembly. *Biomacromolecules* **2015**, *16*, 1433−1441.
(33) Jiang, F.; Hsieh, Y.-L. Amphiphilic Superabsorbent Cellulose Nanofibril Aerogels. *J. Mater. Chem. A* **2014**, *2*, 6337−6342.
(34) Saito, T. Self-Aligned Integration of Native Cellulose Nanofibrils towards Producing Diverse Bulk Materials. *Soft Matter* **2011**, *7*, 8804−8809.
(35) Jiang, F.; Hsieh, Y.-L. Super water absorbing and shape memory nanocellulose aerogels from TEMPO-oxidized cellulose nanofibrils via cyclic freezing-thawing. *J. Mater. Chem. A* **2014**, *2*, 350−359.
(36) Håkansson, K. M. O.; Fall, A. B.; Lundell, F.; Yu, S.; Krywka, C.; Roth, S. V.; Santoro, G.; Kvick, M.; Prahl Wittberg, L.; Wågberg, L.; Söderberg, L. D. Hydrodynamic Alignment and Assembly of Nanofibrils Resulting in Strong Cellulose Filaments. *Nat. Commun.* **2014**, *5*, 1−10.
(37) Liu, A.; Medina, L.; Berglund, L. A. High-Strength Nanocomposite Aerogels of Ternary Composition: Poly(Vinyl Alcohol), Clay, and Cellulose Nanofibrils. *ACS Appl. Mater. Interfaces* **2017**, *9*, 6453−6461.
(38) Tang, H.; Butchosa, N.; Zhou, Q. A Transparent, Hazy, and Strong Macroscopic Ribbon of Oriented Cellulose Nanofibrils Bearing Poly(Ethylene Glycol). *Adv. Mater.* **2015**, *27*, 2070−2076.
(39) Xiong, R.; Kim, H. S.; Zhang, S.; Kim, S.; Korolovych, V. F.; Ma, R.; Yingling, Y. G.; Lu, C.; Tsukruk, V. V. Template-Guided Assembly of Silk Fibroin on Cellulose Nanofibers for Robust Nanostructures with Ultrafast Water Transport. *ACS Nano* **2017**, *11*, 12008−12019.
(40) Xu, X.; Zhou, J.; Jiang, L.; Lubineau, G.; Ng, T.; Ooi, B. S.; Liao, H.-Y.; Shen, C.; Chen, L.; Zhu, J. Y. Highly Transparent, Low-Haze, Hybrid Cellulose Nanopaper as Electrodes for Flexible Electronics. *Nanoscale* **2016**, *8*, 12294−12306.
(41) Mu, X.; Gray, D. G. Formation of Chiral Nematic Films from Cellulose Nanocrystal Suspensions Is a Two-Stage Process. *Langmuir* **2014**, *30*, 9256−9260.
(42) Mu, X.; Gray, D. G. Droplets of cellulose nanocrystal suspensions on drying give iridescent 3-D ″coffee-stain″ rings. *Cellulose* **2015**, *22*, 1103−1107.
(43) Shopsowitz, K. E.; Kelly, J. A.; Hamad, W. Y.; MacLachlan, M. J. Biopolymer Templated Glass with a Twist: Controlling the Chirality, Porosity, and Photonic Properties of Silica with Cellulose Nanocrystals. *Adv. Funct. Mater.* **2014**, *24*, 327−338.
(44) Gu, M.; Jiang, C.; Liu, D.; Prempeh, N.; Smalyukh, I. I. Cellulose Nanocrystal/Poly(Ethylene Glycol) Composite as an Iridescent Coating on Polymer Substrates: Structure-Color and Interface Adhesion. *ACS Appl. Mater. Interfaces* **2016**, *8*, 32565−32573.
(45) Cheung, C. C. Y.; Giese, M.; Kelly, J. A.; Hamad, W. Y.; Maclachlan, M. J. Iridescent Chiral Nematic Cellulose Nanocrystal/Polymer Composites Assembled in Organic Solvents. *ACS Macro Lett.* **2013**, *2*, 1016−1020.
(46) Liu, Q.; Campbell, M. G.; Evans, J. S.; Smalyukh, I. I. Orientationally Ordered Colloidal Co-Dispersions of Gold Nanorods and Cellulose Nanocrystals. *Adv. Mater.* **2014**, *26*, 7178−7184.
(47) De La Cruz, J. A.; Liu, Q.; Senyuk, B.; Frazier, A. W.; Peddireddy, K.; Smalyukh, I. I. Cellulose-Based Reflective Liquid Crystal Films as Optical Filters and Solar Gain Regulators. *ACS Photonics* **2018**, *5*, 2468−2477.
(48) Gu, J.; Hsieh, Y.-L. Surface and Structure Characteristics, Self-Assembling, and Solvent Compatibility of Holocellulose Nanofibrils. *ACS Appl. Mater. Interfaces* **2015**, *7*, 4192−4201.
(49) Jiang, F.; Hsieh, Y.-L. Amphiphilic Superabsorbent Cellulose Nanofibril Aerogels. *J. Mater. Chem. A* **2014**, *2*, 6337−6342.
(50) Xu, X.; Zhou, J.; Xin, Y.; Lubineau, G.; Ma, Q.; Jiang, L. Alcohol Recognition by Flexible, Transparent and Highly Sensitive Graphene-Based Thin-Film Sensors. *Sci. Rep.* **2017**, *7*, 4317.

https://dx.doi.org/10.1021/acsabm.0c00463
ACS Appl. Bio Mater. 2020, 3, 4522−4530

(51) Chen, R.; Zhang, L.; Zang, D.; Shen, W. Wetting and Drying of Colloidal Droplets: Physics and Pattern Formation. *Advances in Colloid Science Patterns*, IntechOpen Limited: London, UK, 2017.
(52) Dai, H.; Ding, R.; Li, M.; Huang, J.; Li, Y.; Trevor, M. Ordering Ag Nanowire Arrays by Spontaneous Spreading of Volatile Droplet on Solid Surface. *Sci. Rep.* **2014**, *4*, 1−5.
(53) Deegan, R. D.; Bakajin, O.; Dupont, T. F.; Huber, G.; Nagel, S. R.; Witten, T. A. Capillary Flow as the Cause of Ring Stains from Dried Liquid Drops. *Nature* **1997**, *389*, 827−829.
(54) Favier, V.; Cavaille, J. Y.; Canova, G. R.; Shrivastava, S. C. Mechanical Percolation in Cellulose Whisker Nanocomposites. *Polym. Eng. Sci.* **1997**, *37*, 1732−1739.

https://dx.doi.org/10.1021/acsabm.0c00463
ACS Appl. Bio Mater. 2020, 3, 4522−4530